energies

MDPI

Article

A Low EMI DC-DC Buck Converter with a Triangular Spread-Spectrum Mechanism

Jing-Yuan Lin, Yi-Chieh Hsu * and Yo-Da Lin

Department of Electronic Engineering, National Taiwan University of Science and Technology, Taipei 106, Taiwan; jylin@mail.ntust.edu.tw (J.-Y.L.); boybobo063@gmail.com (Y.-D.L.)

* Correspondence: D02943003@ntu.edu.tw; Tel.: +886-2-733-3141

Received: 27 December 2019; Accepted: 14 February 2020; Published: 15 February 2020



Abstract: In this paper, a triangular spread-spectrum mechanism is proposed to suppress the electromagnetic interference (EMI) of a DC-DC buck converter. The proposed triangular spread-spectrum mechanism, which is implemented in the chip, can avoid modifying the printed circuit board of switching regulators. In addition, a lower ripple of output voltage of switching regulators and a better system stability can be realized by the inductive DC resistance (DCR) current sensing circuit. The chip is fabricated by using TSMC 0.18-μm 1P6M CMOS technology. The chip area including PADs is 1.2×1.15 mm^2. The input voltage range is 2.7~3.3 V and the output voltage is 1.8 V. The maximum load current is 700 mA. The off-chip inductor and capacitor are 3.3 μH and 10 μF, respectively. The experimental results demonstrate that the maximum spur of the proposed DC-DC buck converter with the triangular spread-spectrum mechanism improves to 14dBm. Moreover, the transient recovery time of step-up and step-down loads are both 5 μs. The measured maximum efficiency is 94% when the load current is 200 mA.

Keywords: constant on-time control; electromagnetic interference; spread-spectrum mechanism; buck converter

1. Introduction

In recent years, portable electronic devices have become an indispensable necessity in daily life. Power management integrated circuits (PMICs) are widely used in portable electronic devices such as smart phones, tablets, laptops, and digital cameras. These products are constantly being updated to make them more practical and convenient. In general, fixed operating frequency control and variable operating frequency control are used in the switching regulator. Switching regulators with fixed operating frequency include both voltage mode control [1,2] and current control mode [3–5]. Fixed operating frequency control mechanisms must utilize an error amplifier and additional compensation components to stabilize the output voltage of the DC-DC buck converter. Another type of control scheme is variable operating frequency control, including hysteresis control [6–8] and constant on-time control [9–11]. First, the hysteresis control is controlled by the ripple of output voltage of the DC-DC buck converter. When the ripple of output voltage is higher than the upper threshold voltage or lower than the lower threshold voltage, the control circuit will generate a corresponding switching signal to drive power transistors. In addition, to stabilize the system it is necessary to use a capacitor with large equivalent series resistance (ESR) as an output capacitor of the DC-DC buck converter, such as an electrolytic capacitor. The constant on-time control is another control method, as shown in Figure 1. When the output voltage of the DC-DC buck converter is lower than the reference voltage, the power transistors are controlled with a fixed on-time. This method also needs to be controlled by the ripple of output voltage of the DC-DC buck converter, so it is also necessary to use an electrolytic capacitor as an output capacitor of the DC-DC buck converter to stabilize the system.

Compared with electrolytic capacitors, a multilayer ceramic capacitor (MLCC) has the advantages of long used time, low cost, better high frequency response, and small size. However, the use of an MLCC as the output capacitor of a DC-DC buck converter in a variable operating frequency system must be accompanied by additional control mechanisms to maintain system stability. Hence, there are some studies that propose a combination of low ripple of output voltage and system stability [12,13]. In addition, since the variable frequency control system has a gradually increasing switching loss ratio of the power transistor at a light load, the constant on-time control can improve the efficiency of the DC-DC buck converter by lowering the operating frequency.

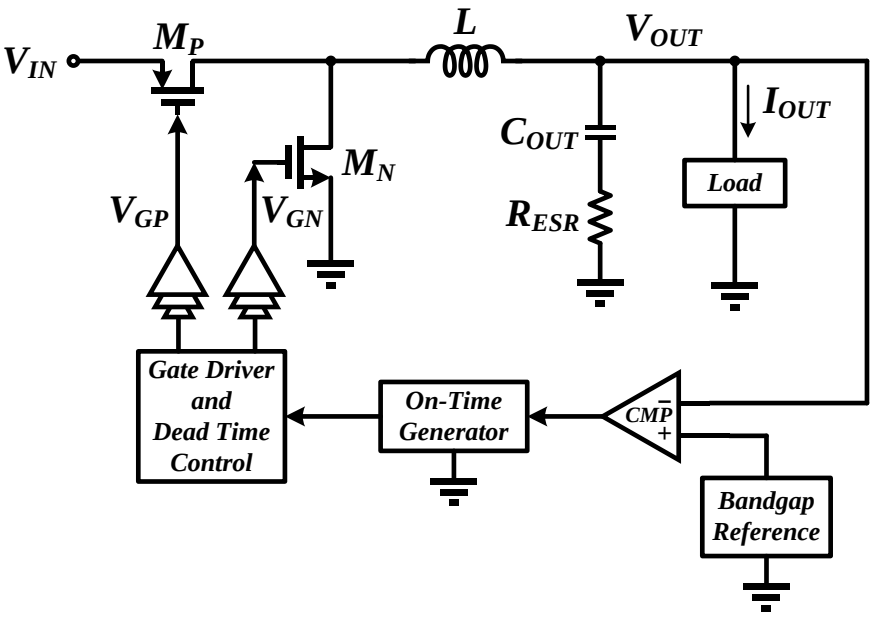

Figure 1. Schematic of the constant on-time DC-DC buck converter.

Switching regulators have many advantages, such as high conversion efficiency and small size. However, there are still some shortcomings that must be carefully considered, the most important of which is the electromagnetic interference (EMI) of the DC-DC buck converter [14–16]. Figure 2 shows the EMI of a portable electronic device. EMI is an electromagnetic noise that is not conducive to other systems during the normal operation of a DC-DC buck converter, which is a serious problem for safety regulations. Therefore, in order to eliminate the influence of EMI, it is necessary to modify the layout of the printed circuit board of the switching regulators or to add additional control circuits, which will increase the cost of the product. Random switching frequency is one of the most effective ways to reduce EMI [17]. This method disperses the power of spurs of the converter in the frequency domain by randomly adjusting the switching frequency. However, the disadvantage is that the instantaneous jitter of the switching frequency is too large, which will increase the ripple of the output voltage. To suppress the EMI of the DC-DC buck converter and the ripple of output voltage, the triangular spread-spectrum mechanism is presented in this paper. The EMI of the DC-DC buck converter is introduced in Section 2. The circuit implementation of the proposed triangular spread-spectrum mechanism is described in Section 3. Finally, the experimental results and conclusions are shown in Sections 4 and 5, respectively.

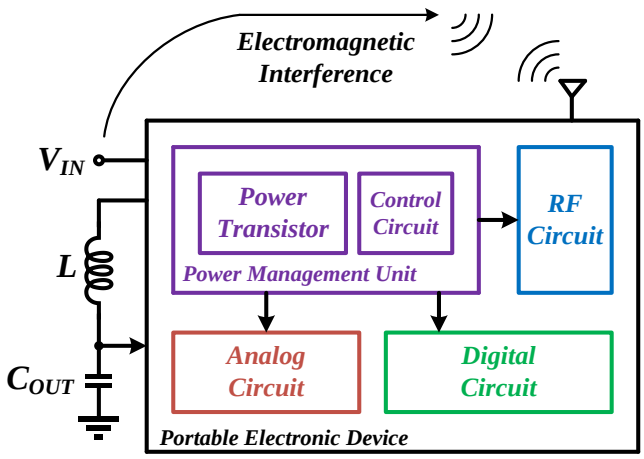

Figure 2. Electromagnetic interference of the portable electronic device.

2. Electromagnetic Interference of the DC-DC Buck Converter

Electromagnetic compatibility (EMC) is a very important issue for switching regulators. If the standard of EMC is not taken into account in the design of the switching regulator, it will take more time to deal with the effects of EMI, such as modifying the layout of the printed circuit board of the switching regulators.

Figure 3 depicts the inductor current distribution of the DC-DC buck converter. There are two dramatically varying current loops (I_1 and I_2) in the DC-DC buck converter. First, when the power transistor M_p is turned on, the current loop I_1 passes through the input voltage V_{IN}, the power transistor M_p, the inductor L, the output capacitor C_{OUT}, and the load. Next, in order to maintain the continuity of the inductor current, the power transistor M_n will be turned on. The current loop I_2 flows through the power transistor M_n, the inductor L, the output capacitor C_{OUT}, and the load at this time. According to the operating principle of the switching regulator, we can find that the current loops I_1 and I_2 are not continuous. This will therefore cause a large current change rate, resulting in the generation of high frequency components. There are two areas (A_1 and A_2) included in the inductor current distribution of the DC-DC buck converter. The area A_1 has a large high frequency component because only the current loop I_1 passes. On the other hand, since both current loops I_1 and I_2 pass through the area A_2, the inductor current forms a smooth and continuous triangular wave. Thus, the high frequency component of the area A_2 is reduced. In summary, the EMI of area A_1 will be higher than the area A_2. As a result, the input terminal of the DC-DC buck converter will generate a large EMI. Consequently, the EMI of the DC-DC buck convertor can be suppressed by the spread-spectrum technique, as shown in Figure 4.

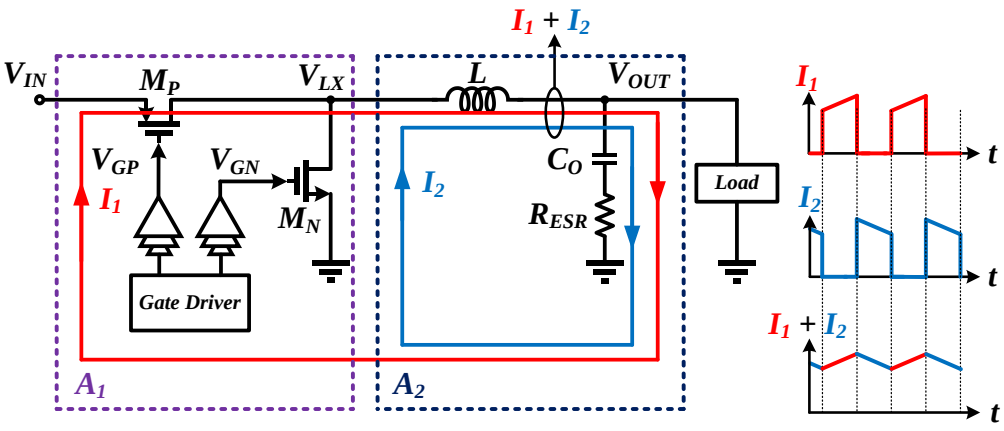

Figure 3. Inductor current distribution of the DC-DC buck converter.

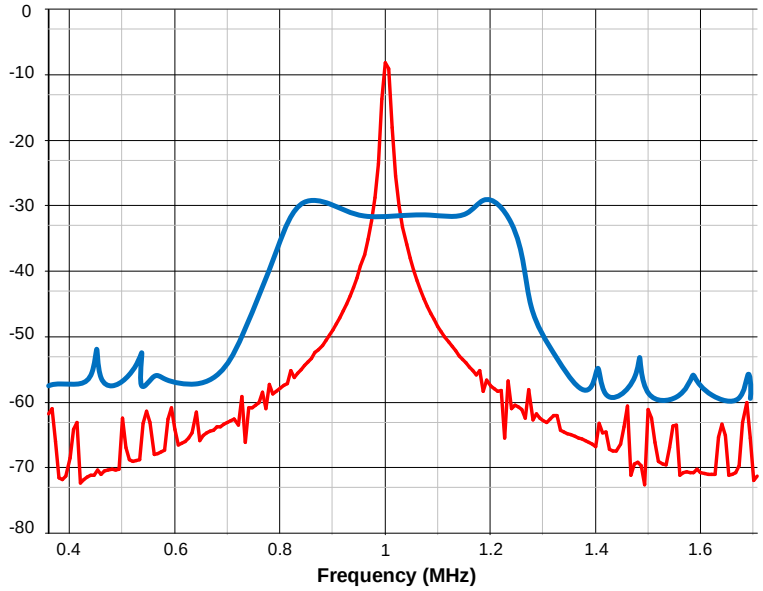

Figure 4. Spectrum waveform with and without spread-spectrum technique.

3. Circuit Implementation

The triangular spread-spectrum mechanism proposed in this paper uses a triangular wave to modulate the on-time of the power transistor. Due to the switching frequency being gradually increased or decreased, the waveform of the inductor current is smoother. In addition, reducing the ripple of output voltage can also make the output voltage of the converter more stable. The block diagram of the proposed DC-DC buck converter is shown in Figure 5. To realize the spur reduction, this paper proposes a low EMI DC-DC buck converter with a triangular spread-spectrum mechanism that effectively mitigates the effects of EMI. In addition, the system stability and the ripple of the DC-DC buck converter are improved by the inductive DC resistance (DCR) current sensing circuit.

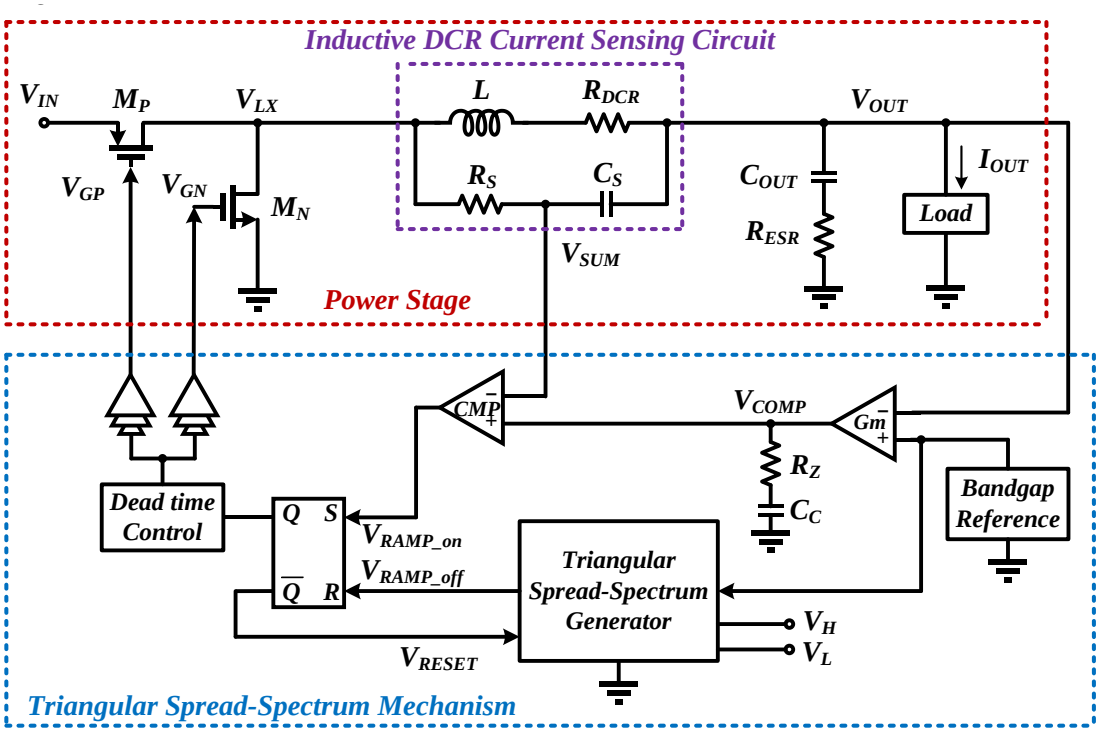

Figure 5. Block diagram of the proposed DC-DC buck converter.

3.1. Proposed Triangular Spread-Spectrum Generator

The schematic of the proposed triangular spread-spectrum generator and simulation waveform are shown in Figures 6 and 7, respectively. The triangular spread-spectrum generator is composed of a triangular wave generator and an on-time generator. First, the triangular wave generator includes current sources I_1 and I_2, a capacitor C_1, comparators CMP_1 and CMP_2, an SR latch, and transistors M_1-M_4. Assuming that the initial voltage of the capacitor C_1 is 0V, the SR latch will provide a high-level voltage to turn off the transistor M_1. Thus, the current source I_1 will charge the capacitor C_1. When the voltage of the capacitor C_1 is higher than the upper threshold voltage V_H, a low-level voltage will be produced by the SR latch to turn on the transistor M_1. If the current source I_1 is designed to be half of the current source I_2, the capacitor C_1 will be discharged through the transistors M_3 and M_4 and the current source I_2. When the voltage of the capacitor C_1 is lower than the lower threshold voltage V_L, the current source I_1 will charge the capacitor C_1 again. By repeating the above operation, a triangular wave V_{TRI} can be obtained. In general, the upper threshold voltage V_H and the lower threshold voltage V_L will affect the slope of the triangular wave. Thus, it would appear that a smoother triangular wave has a smaller impact on the output voltage, that is, it has a lower ripple of output voltage and a smooth output voltage. Next, the on-time generator comprises a current source I_3, a comparator CMP_3, a capacitor C_2, and transistors M_5-M_9. The current source I_3 charges the capacitor C_2 via the transistors M_5-M_8. When the voltage of the capacitor C_2 is higher than the triangular wave V_{TRI}, the comparator CMP_3 will generate a pulse signal to the SR latch to modulate the on-time. The voltage of the capacitor C_2 will be discharged at this time by using the transistor M_9.

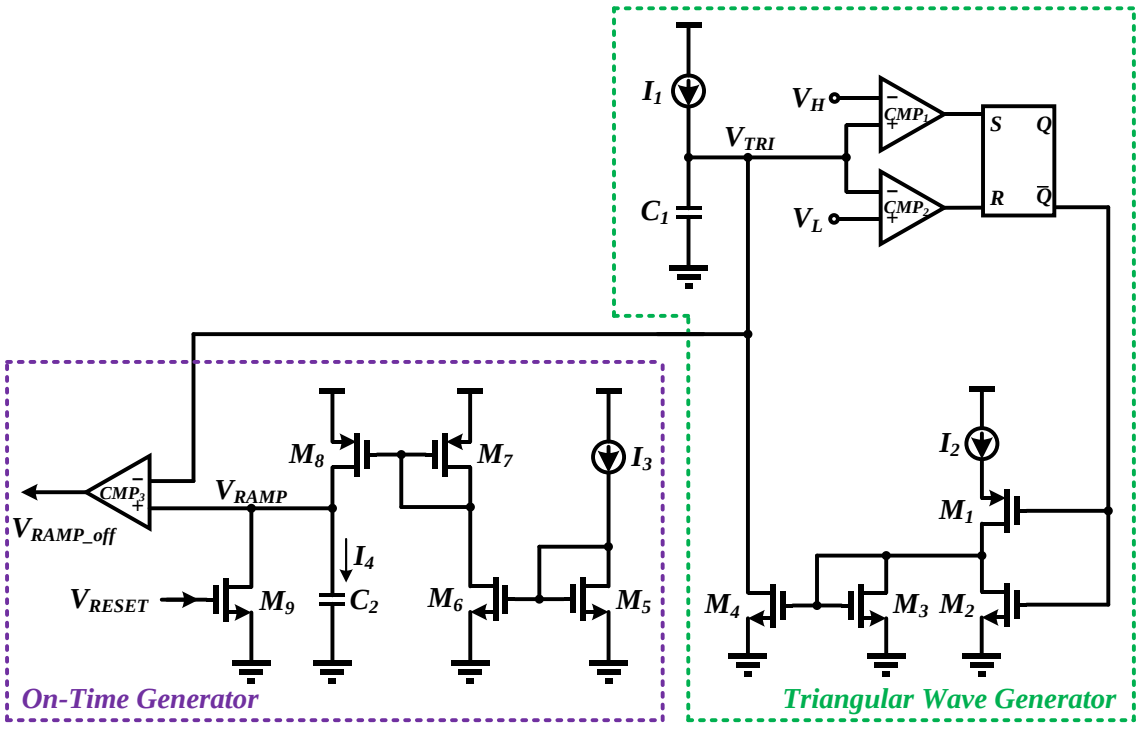

Figure 6. Schematic of the proposed triangular spread-spectrum generator.

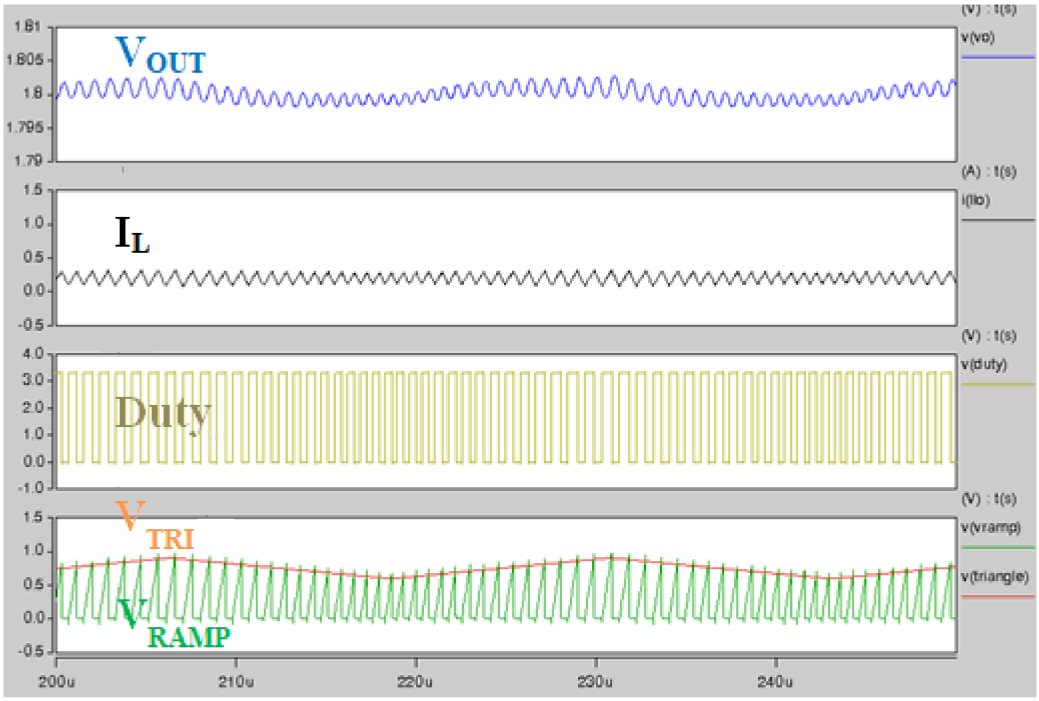

Figure 7. Simulation waveform of the triangular spread-spectrum generator.

3.2. Inductive DCR Current Sensing Circuit

The inductive DCR current sensing circuit is depicted in Figure 8. Due to the reduced ripple of output voltage of the DC-DC buck converter, the output capacitor with low ESR is employed. However, lower ripple of output voltage of the DC-DC buck converter causes system instability. Thus, to prevent sensing incorrect information on the inductor current, the inductive DCR current sensing circuit is adopted to obtain information on the inductor current. It is composed of an inductor with DCR R_{DCR} and filter circuits R_S and C_S. The operating principle of the inductive DCR current sensing circuit is to sense the inductor current by the inductive DCR R_{DCR} and obtain the sensing voltage V_{SEN} through the filter circuits R_S and C_S. It can be expressed as

$$V_{sen}(s) = \frac{i_L(R_{dcr} + sL)}{1 + sR_sC_s} = (i_L R_{dcr})[\frac{1 + s\left(\frac{L}{R_{dcr}}\right)}{1 + sR_sC_s}] \quad (1)$$

When the time constants in Equation (1) are equal, it can be determined as

$$R_sC_s = \frac{L}{R_{dcr}} \quad (2)$$

By substituting Equation (2) into Equation (1), V_{SEN} can be simplified as

$$V_{sen}(s) = i_L R_{dcr} \quad (3)$$

The output voltage of the inductive DCR current sensing circuit V_{SUM} can be calculated as

$$V_{sum}(s) = V_{out} + V_{sen}(s) \quad (4)$$

It can be found from Equation (4) that the output voltage of the inductive DCR current sensing circuit V_{SUM} is composed of the output voltage of the DC-DC buck converter V_{OUT} and the sensing voltage V_{SEN}. Thus, even if the MLCC is used as the output capacitor C_{OUT}, the output voltage of the inductive DCR current sensing circuit V_{SUM} can acquire the correct information on the inductor current.

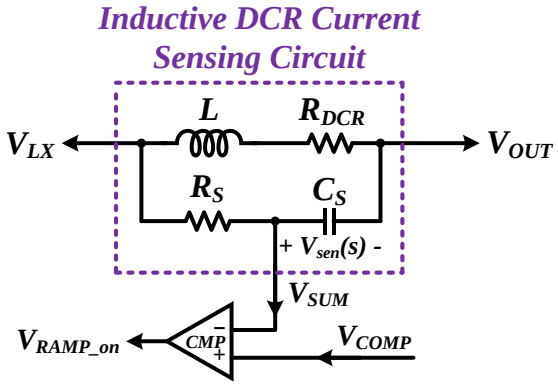

Figure 8. Schematic of the inductive DC resistance (DCR) current sensing circuit.

4. Experimental Results

In order to verify the proposed DC-DC buck converter with the triangular spread-spectrum mechanism, the chip is implemented using TSMC 1P6M 0.18-μm CMOS technology. The chip microphotograph is shown in Figure 9, and consists of the power transistors, gate driver and proposed triangular spread-spectrum mechanism.

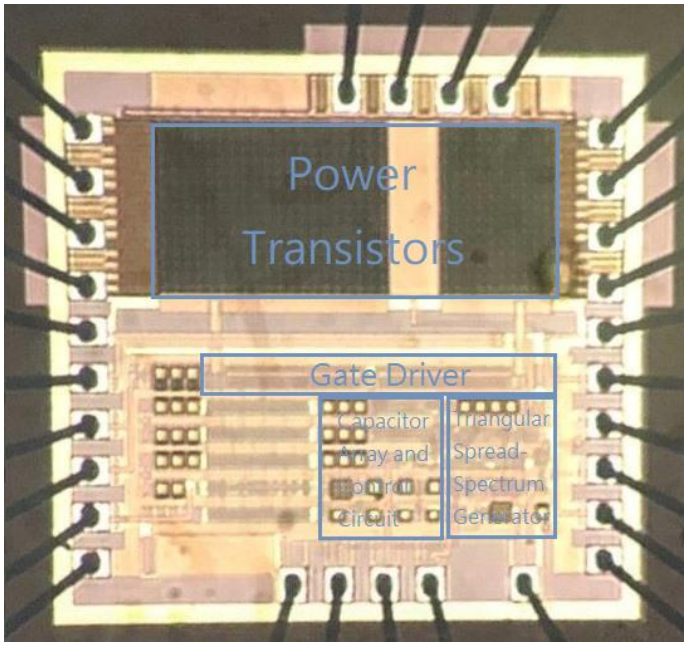

Figure 9. Chip microphotograph.

The chip area including PADs is 1.2×1.15 mm^2. The off-chip inductor and capacitor are adopted as 3.3 μH and 10 μF, respectively. The operating frequency ranges from 0.7 MHz to 1.3 MHz. The nominal input voltage and output voltage are 3.3 V and 1.8 V, respectively. The maximum load current is 700 mA. The experimental results are shown in Figures 10–19, including the steady-state response, ripple of output voltage, transient recovery time, spectrum waveform and conversion efficiency.

Figures 10 and 11 show the measured results of the light load (I_{LOAD} = 200 mA) and the heavy load (I_{LOAD} = 700 mA) steady-state response of the proposed DC-DC buck converter, respectively. The measured results include the output voltage V_{OUT} of the DC-DC buck converter, the connection of the power transistors V_{LX} and the inductor current I_L. It can be found that the output voltages of the proposed DC-DC buck converter are both 1.8 V from the measured results.

The light load (I_{LOAD} = 200 mA) and heavy load (I_{LOAD} = 700 mA) output ripples of the proposed DC-DC buck converter, as shown in Figures 12 and 13, are both less than 3 mV.

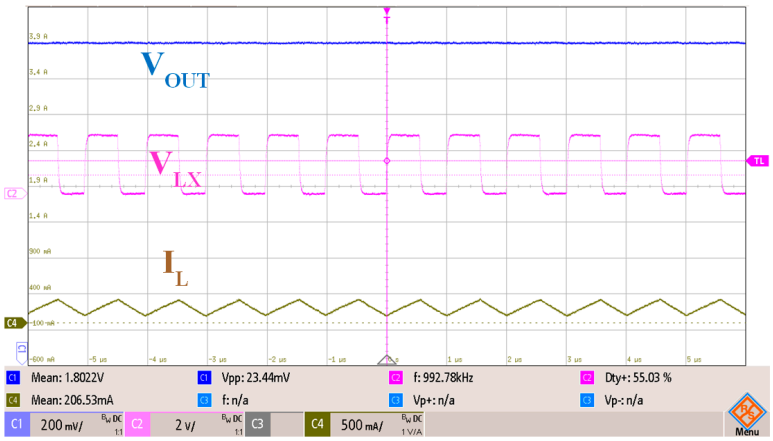

Figure 10. Measured light load steady-state response of the proposed DC-DC buck converter (V_{OUT} = 1.8 V; I_{LOAD} = 200 mA).

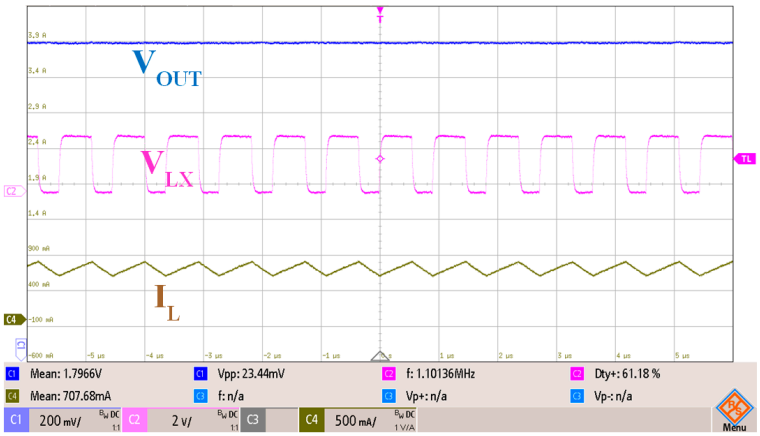

Figure 11. Measured heavy load steady-state response of the proposed DC-DC buck converter (V_{OUT} = 1.8 V; I_{LOAD} = 700 mA).

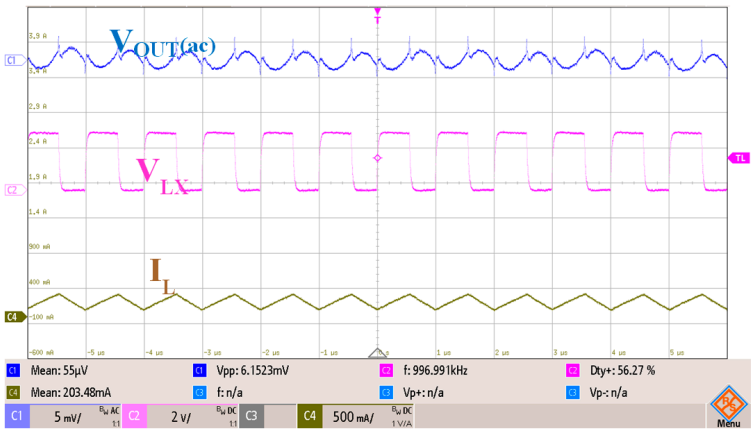

Figure 12. Measured light load output ripple of the proposed DC-DC buck converter (V_{OUT} = 1.8 V; I_{LOAD} = 200 mA).

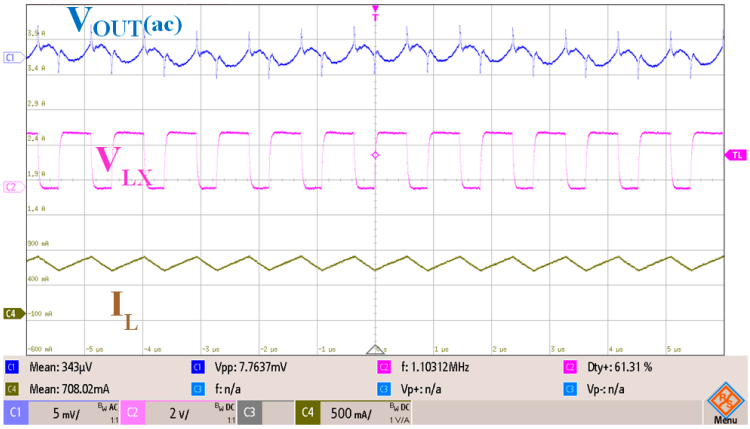

Figure 13. Measured heavy load output ripple of the proposed DC-DC buck converter (V_{OUT} = 1.8 V; I_{LOAD} = 700 mA).

The measured transient response of the proposed DC-DC buck converter is shown in Figure 14. Figures 15 and 16 depict the transient recovery times for the step-up and step-down loads of the proposed DC-DC buck converter, respectively. According to the measured results, the transient recovery time of the proposed DC-DC buck converter is 5µs for both step-up (from I_{LOAD} = 200 mA to I_{LOAD} = 700 mA) and step-down (from I_{LOAD} = 700 mA to I_{LOAD} = 200 mA) loads.

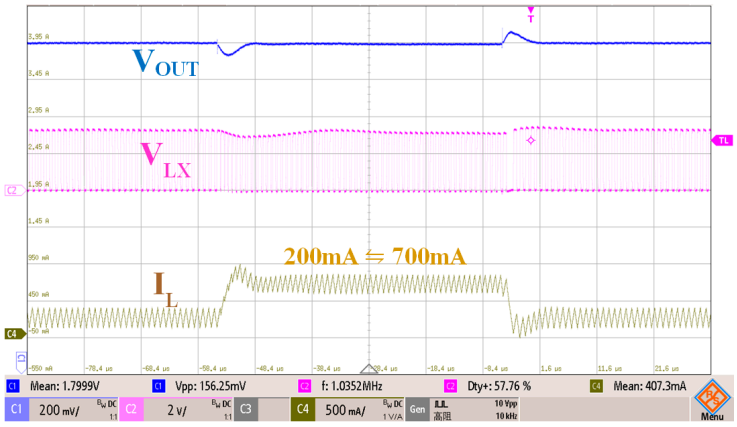

Figure 14. Measured transient response of the proposed DC-DC buck converter.

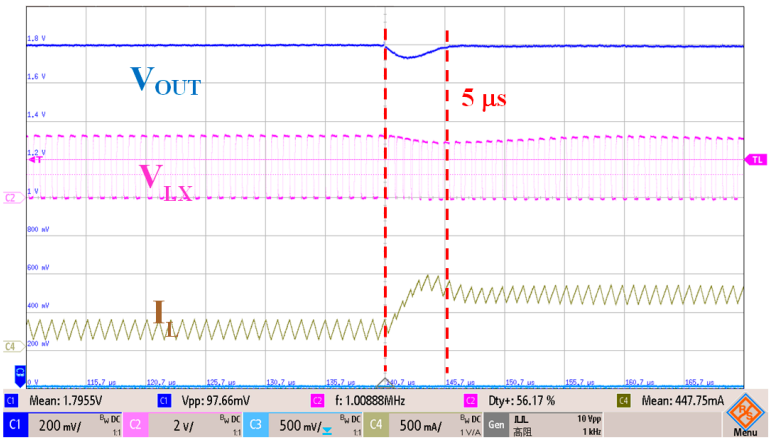

Figure 15. Measured transient recovery time with the proposed DC-DC buck converter for a step-up load from 200 mA to 700 mA.

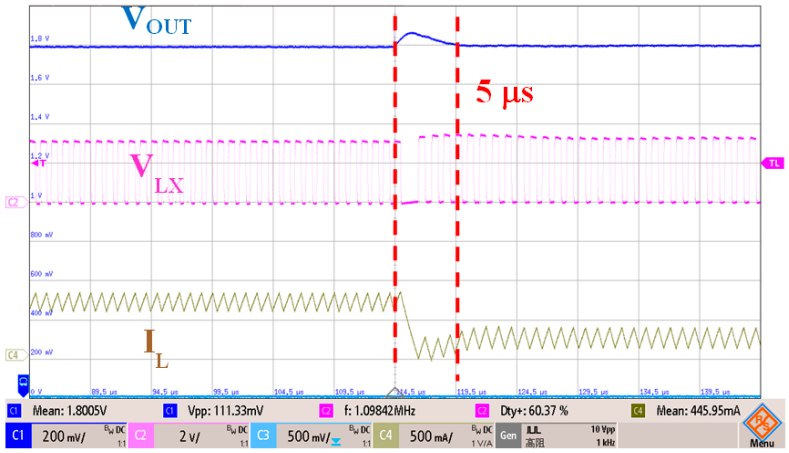

Figure 16. Measured transient recovery time with the proposed DC-DC buck converter for a step-down load from 200 mA to 700 mA.

The measured spectrum waveforms of the Fast Fourier Transform (FFT) without and with the proposed triangular spread-spectrum mechanism are shown in Figures 17 and 18, respectively. The measured maximum spurs of the DC-DC buck converter without and with the proposed triangular spread-spectrum mechanism are −46 dBm and −60 dBm, respectively. The experimental results show that the maximum spur of the proposed DC-DC buck converter with the triangular spread-spectrum mechanism improved by 14 dBm. The measured efficiency of the proposed DC-DC buck converter is illustrated in Figure 19. The maximum conversion efficiency is 94% when the load current is 200 mA. The specification of the proposed DC-DC buck converter with the triangular spread-spectrum mechanism is listed in Table 1.

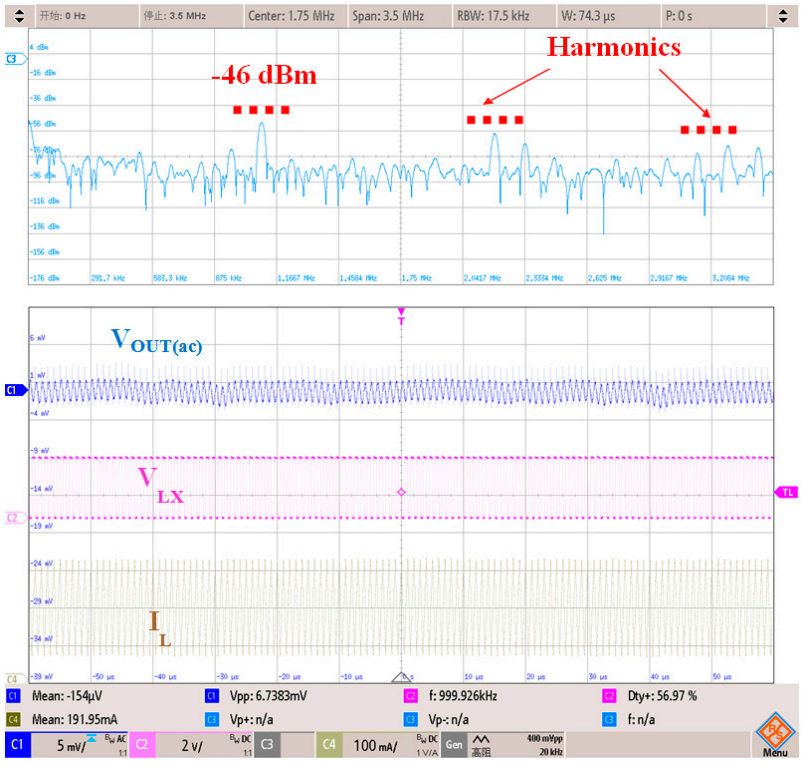

Figure 17. Measured spectrum waveform without the proposed triangular spread-spectrum mechanism.

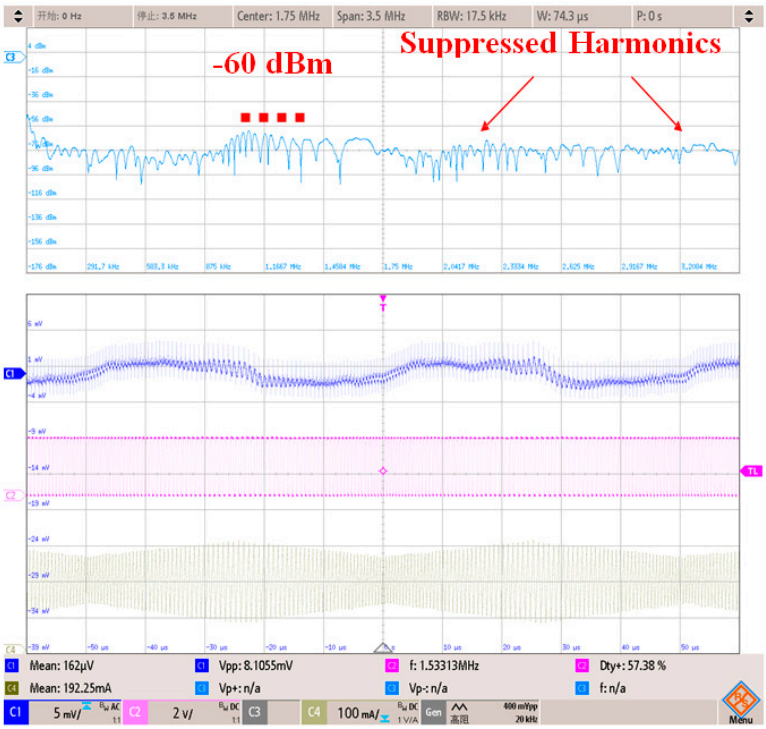

Figure 18. Measured spectrum waveform with the proposed triangular spread-spectrum mechanism.

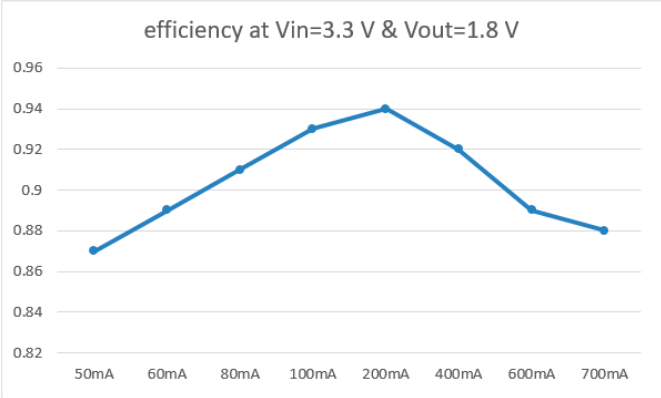

Figure 19. Measured conversion efficiency of the proposed DC-DC buck converter.

Table 1. Specification of the proposed DC-DC buck converter.

Parameter	This Work
Technology (nm)	**180**
Control scheme	**Constant on-time**
Switching frequency (MHz)	**0.7~1.3**
Input voltage (V)	**2.9~3.3**
Output voltage (V)	**1.8**
Inductor (µH)/Capacitor (µF)	**3.3/10**
Peak efficiency (%)	**94**
Load current (mA)	**50~700**
Transient recovery time for step-up load (µs)	**5**
Transient recovery time for step-down load (µs)	**5**
Chip area (mm^2)	**1.38**

5. Conclusions

This paper presents the possibility of a low EMI DC-DC buck converter with a triangular spread-spectrum mechanism to reduce the EMI. The proposed triangular spread-spectrum mechanism is implemented in the chip, so there is no need to modify the PCB in order to mitigate the effect of EMI. On the other hand, reducing the ripple of output voltage of the DC-DC buck converter and maintaining system stability can be realized by the inductive DCR current sensing circuit. The chip is implemented by using the TSMC 0.18-μm 1P6M CMOS process. The chip area including PADs is 1.2×1.15 mm^2. The input voltage range is 2.7–3.3 V and output voltage is 1.8 V. The maximum load current is 700 mA. The off-chip inductor and capacitor are 3.3 μH and 10 μF, respectively. The measured results show that the maximum spur of the proposed DC-DC buck converter with a triangular spread-spectrum mechanism is suppressed to 14 dBm. Moreover, the transient recovery time of step-up and step-down loads are both 5 μs. The measured efficiency is 94% when the load current is 200 mA.

Author Contributions: J.-Y.L. and Y.-C.H. conceived and designed the architecture and experiment. Y.-D.L. performed the experiment. Y.-C.H. wrote the paper. J.-Y.L. provided all material for the experiment, and supervised the design, analysis, experiment, and editing of the paper. All authors have read and agreed to the published version of the manuscript.

Funding: This research received no external funding.

Acknowledgments: The authors would like to thank the Taiwan Semiconductor Research Institute (TSRI) for chip fabrication and technical support.

Conflicts of Interest: The authors declare no conflict of interest.

References

1. Hsu, Y.-C.; Ting, C.-Y.; Hsu, L.-H.; Lin, J.-Y.; Chen, C.-P. A transient enhancement DC-DC buck converter using dual operating mode control technique. *IEEE Trans. Circuits Syst. II Exp. Briefs* **2018**, *66*, 1376–1380. [CrossRef]
2. Suh, J.-D.; Seok, J.; Kong, B.-S. A fast response PWM buck converter with active ramp tracking control in load transient period. *IEEE Trans. Circuits Syst. II Exp. Briefs* **2018**, *66*, 467–471. [CrossRef]
3. Lee, C.-F.; Mok, P.-K.-T. A monolithic current-mode CMOS DC-DC converter with on-chip current-sensing technique. *IEEE J. Solid State Circuits* **2004**, *39*, 3–14. [CrossRef]
4. Wu, K.-I.; Hwang, B.-T.; Chen, C.-P. Synchronous double-pumping technique for integrated current-mode PWM DC–DC converters demand on fast-transient response. *IEEE Trans. Power Electron.* **2017**, *32*, 849–865. [CrossRef]
5. Lee, Y.-H.; Huang, S.-C.; Wang, S.-W.; Chen, K.-H. Fast transient (FT) technique with adaptive phase margin (APM) for current mode DC–DC buck converters. *IEEE Trans. Very Large Scale Integr. (VLSI) Syst.* **2012**, *20*, 1781–1793. [CrossRef]
6. Huang, H.-H.; Chen, C.-L.; Chen, K.-H. Adaptive window control (AWC) technique for hysteresis DC-DC buck converters with improved light and heavy load performance. *IEEE Trans. Power Electron.* **2009**, *24*, 1607–1617. [CrossRef]
7. Wu, K.-I.; Hung, S.-H.; Shieh, S.-Y.; Hwang, B.-T.; Hung, S.-Y.; Chen, C.C.-P. Current-mode adaptively hysteretic control for buck converters with fast transient response and improved output regulation. In Proceedings of the IEEE International Symposium on Circuits and Systems (ISCAS), Melbourne, Australia, 1–5 June 2014; pp. 950–953.
8. Hwang, Y.-S.; Wu, T.-H.; Lu, M.-X.; Chen, J.-J. Sub-1-V fast-response hysteresis- controlled CMOS buck converter using adaptive ramp techniques. *IEEE Trans. Very Large Scale Integr. (VLSI) Syst.* **2013**, *21*, 1608–1618.
9. Lin, Y.-C.; Chen, C.-J.; Chen, D.; Wang, B. A ripple-based constant on-time control with virtual inductor current and offset cancellation for DC power converters. *IEEE Trans. Power Electron.* **2012**, *27*, 4301–4310. [CrossRef]
10. Chen, W.-W.; Chen, J.-F.; Liang, T.-J.; Wei, L.-C.; Huang, J.-R.; Ting, W.-Y. A novel quick response of RBCOT with VIC ripple for buck converter. *IEEE Trans. Power Electron.* **2013**, *28*, 4299–4307. [CrossRef]

11. Li, C.-H.; Chiu, H.-J.; Lo, Y.-K.; Wang, C.-C. Adaptive on-time control with adjustable virtual ripple and offset cancellation for buck converter. *IET Power Electron.* **2015**, *12*, 2418–2428. [CrossRef]
12. Chen, C.; Chen, D.; Tseng, C.; Chang, Y.; Wang, K. A novel ripple-based constant on time control with virtual inductor current ripple for buck converter with ceramic output capacitors. In Proceedings of the IEEE APEC, San Francisco, CA, USA, 21–25 February 2011; pp. 1488–1493.
13. Chen, W.-C.; Wang, C.-S.; Su, Y.-P.; Lee, Y.-H.; Lin, C.-C.; Chen, K.-H.; Du, M.-J. Reduction of equivalent series inductor effect in delay ripple reshaped constant on-time control for buck converter with multilayer ceramic capacitors. *IEEE Trans. Power Electron.* **2013**, *28*, 2366–2376. [CrossRef]
14. Lee, Y.-H.; Wang, S.-J.; Chen, K.-H. Quadratic differential and integration technique in V^2 control buck converter with small ESR capacitor. *IEEE Trans. Power Electron.* **2010**, *25*, 829–838.
15. Su, Y.-P.; Lee, Y.-H.; Chen, W.-C.; Chen, K.-H.; Lin, Y.-H.; Tsai, T.-Y.; Huang, C.-C.; Lee, C.-C. A pseudo-noise coded constant-off-time (PNC-COT) control switching converter with maximum 18.7-dBm peak spur reduction and 92% efficiency in 40 nm CMOS. In Proceedings of the IEEE Symposium on VLSIC, Kyoto, Japan, 11–14 June 2013; pp. C170–C171.
16. Du, Y.; Liu, Q.; Huang, A.-Q. Current-mode hysteretic buck converter with spur-free control for variable switching noise mitigation. In Proceedings of the ECCE, Raleigh, NC, USA, 15–20 September 2012; pp. 1849–1856.
17. Liu, P.-J.; Tai, J.-N.; Chen, H.-S.; Chen, J.-H.; Chen, Y.-J. Spur-reduction design of frequency-hopping DC–DC converters. *IEEE Trans. Power Electron.* **2012**, *27*, 4763–4771. [CrossRef]



© 2020 by the authors. Licensee MDPI, Basel, Switzerland. This article is an open access article distributed under the terms and conditions of the Creative Commons Attribution (CC BY) license (http://creativecommons.org/licenses/by/4.0/).